18TH WORLD CONFERENCE ON EARTHQUAKE ENGINEERING
WCEE2024
MILAN

MILAN, ITALY
30TH JUNE - 5TH JULY 2024

www.wcee2024.it

MITIGATING SEISMIC VULNERABILITY OF WIND TURBINES USING TUNED MASS DAMPERS AND INERTERS

J. McAuliffe[1], B. Broderick[1], J. Hickey[1] & B. Fitzgerald[1]

[1] Department of Civil, Structural and Environmental Engineering, School of Engineering, Trinity College Dublin, Ireland, jmcaulif@tcd.ie

Abstract: *Seismic loads can cause significant damage to wind turbines, leading to costly repairs and downtime. In this study, we investigate the response of a 150m tall, 15-MW wind turbine to seismic loads and propose a vibration control strategy using tuned mass dampers (TMDs) and tuned mass damper inerters (TMDIs). Inerter-based dampers have recently been applied to improve the seismic performance of structures such as multi-storey buildings and bridges and have been used for vibration control of wind turbines subjected to turbulent aerodynamic loading. Compared to traditional TMDs, TMDIs have been shown to be more effective in reducing structural responses whilst also reducing the damper stroke required for operation and can therefore be used in structures with limited space available for dampers such as wind turbine towers. This study develops a finite element (FE) model of a 15-MW wind turbine. The FE model was constructed using Abaqus software, leveraging Solidworks geometry provided by the International Energy Agency (IEA). The model incorporates detailed representations of the tower, foundation, and blades, utilising a combination of hexahedral and tetrahedral elements to accurately capture their complex geometries. The meshing process involved refining the mesh in critical regions to capture local stress concentrations and deformation patterns. Boundary conditions are carefully defined to capture the dynamic behaviour of the system while considering relevant degrees of freedom and connections between components. The model has been verified via a modal analysis comparing both the first natural frequency and mode shape of the tower with those specified by the IEA. Dynamic time-domain simulations of earthquake records of varying magnitudes and frequencies have been performed using the finite element model and a fragility analysis is presented to demonstrate the clear benefits of installing dampers in wind turbines subjected to seismic loads. The results of the study show that the TMDI controlled structure outperforms the TMD controlled system in terms of reducing the seismic response of the wind turbine. The findings of this study may inform the design of future wind turbines and other large-scale structures in seismic-prone regions. Overall, this study highlights the importance of considering the seismic response of wind turbines and proposes an effective mitigation strategy that can enhance their resilience to seismic events.*

1. Introduction

Over the last two decades, in an endeavour to reduce the levelised cost of energy (LCOE) produced by wind turbines, wind turbine technology has undergone a rapid up-scaling in both the size and ability of wind turbines to capture energy. Enevoldsen and Xydis (2019) detail the extent of this development, reporting that wind turbine hub heights for onshore wind turbines have doubled from 82m in 1998 to 164m in 2016. The effects of wind shear coupled with increased hub heights have allowed wind turbines to capture stronger and less turbulent air flows. In addition to the increased quality of airflow, increasing the hub height of wind turbines has also enabled an increase in rotor diameters. In a similar time frame, wind turbine rotor diameters have almost tripled, increasing from 54m in 1998 to 158m in 2017 (Enevoldsen and Xydis, 2019). Considering that the power produced by wind turbines is related to the cube of the wind speed and the square of the rotor diameter, by increasing both these elements the energy production capacity of individual wind turbines has significantly risen allowing modern wind turbines to be constructed with capacities exceeding 15-MW. However, this

considerable increase in wind turbine scale is not without consequences. Modern multi-mega-watt wind turbines are becoming increasingly slender and flexible structures which in turn makes them extremely vulnerable to horizontal loading arising from wind, waves, and seismic events.

The wide-scale deployment of modern wind turbines has been motivated not only by the reducing LCOE of wind turbines but also by the substantial rise in the cost of energy produced by fossil fuels. Between January 2020 and December 2021 there was a 50% increase in the World Bank energy price index (Justin-Damien, 2022). The impact of geopolitical events leading to energy crises' occurring in recent years has highlighted the importance of energy security to states around the world and has added to the demand for local renewable energy sources such as wind to provide security of supply. As wind turbines are becoming increasingly popular, they are beginning to be installed in seismic-prone regions such as China, India, Japan, South Korea, Europe, Mexico and the USA. California in the USA produces just under 6 GW of electricity from wind turbines annually making it the third-largest wind energy producer in the USA (Katsanos et al., 2016). Due to the high seismicity of California, wind turbines constructed in this region must be capable of resisting seismic loading in order minimise the cost of repairs and to ensure energy security during seismic events. As a result, the seismic reliability of wind turbines located in areas such as California must be closely examined.

In 2010 Prowell et al. (2010) modified the National Renewable Energy Laboratory's (NREL) wind turbine simulator FAST, enabling users to apply base excitations thus allowing for seismic activity to be simulated on wind turbines in both operational and parked states. Yuan et al. (2017) implemented Prowells FAST software to explore the fragility of large-scale wind turbines when experiencing both seismic and aerodynamic loading. This work concluded that the wind loads on the turbine had a low impact on the fragility of the structure in comparison with seismic loads. Additionally, it was found that due to the aerodynamic damping arising during operation, the maximum values of dynamic response were less than the values experienced in the parked condition. This result was mirrored in a similar study by Katsanos et al. (2017) who also explored the dynamic response of the 5-MW NREL offshore wind turbine exposed to seismic and wind loads. Katsanos came to a similar conclusion that the dynamic response of the turbine tower was heavily influenced by seismic loads in comparison with wind loads.

Finite element analysis can be used to improve our understanding of wind turbine's responses under seismic motions as it can more accurately capture the nonlinear nature of the responses. Asareh et al. (2016) developed a finite element model of NRELs 5-MW wind turbine via Abaqus software which allowed for a fragility analysis of the turbine subject to seismic motion to be performed. A similar result to Katsanos and Yuan's findings were echoed, concluding that the wind loading had a reduced effect on the dynamic behaviour of the wind turbine in comparison with the seismic motions applied. Mo et al. (2017) similarly performed a fragility analysis of NRELs 5-MW wind turbine using a finite element model on OpenSees. It was noted that the frequency of the input ground motion has a high influence on the response of the structure. Yeter et al. (2020) carried out a fragility analysis on an aging model of a 5-MW monopile-based wind turbine taking into account non-uniform corrosion degradation. The study found that the turbine displacements before failure displayed similarities to the first and second mode shapes of the tower. Del Campo and Pozos-Estrada (2020) performed a fragility analysis of NRELs 5-MW turbine under wind and seismic loading in the Southwest of Mexico using ANSYS. It was concluded that when in the operational state, wind loads dominate the response, while in the parked condition seismic loads become dominant.

In an attempt to reduce displacements and accelerations experienced by large flexible wind turbines, designers have begun implementing damping devices such as the tuned mass damper (TMD). The use of TMDs in wind turbines to mitigate dynamic responses due to wind and waves has been investigated in depth (Murtagh et al., 2008; Lackner and Rotea, 2011a; Si et al., 2013; Stewart and Lackner, 2014; Martin del Campo et al., 2021). The capability of TMD devices to reduce seismic responses of wind turbines have also been explored by (Hoang et al., 2008; Dyke et al., 1995; Zuo et al., 2017; Zhao et al., 2018; Li et al., 2020; Martin del Campo et al., 2021; Dai et al., 2021; Kontoni and Farghaly, 2023) proving the device capable of seismic response control by reducing loads and displacements induced in wind turbines. Despite these positive results, the large mass ratios required coupled with limited effective frequency ranges render the TMD as a substandard vibration controller for offshore wind turbines (Fitzgerald and Basu, 2020). Research on numerous variations and adaptations of the TMD have been carried out in an effort to overcome the deficiencies of the traditional TMD including active TMDs (Lackner and Rotea, 2011b; Fitzgerald et al., 2013; Fitzgerald et al., 2018), semi-active TMDs (Arrigan et al., 2011) and tuned liquid column dampers (Sarkar and Chakraborty, 2018). In 2002 (Smith,

2002) introduced the inerter device that enabled the concept and later the development of the novel Tuned Mass Damper Inerter (TMDI). An inerter is a mechanical device that converts linear motion into high-speed rotational motion. When placed in parallel to the spring and viscous dampers in a TMD, the inerter acts to amplify the effective mass of the TMD. The addition of the inerter enables increased response control at given mass ratios and allows the device to function effectively over a wider range of frequencies. The introduction of inerters into damping devices in an effort to reduce the seismic response of the structures has been examined widely via both experimental testing and numerical analysis reporting the benefits of installing the inerter device in vulnerable structures (De Domenico et al., 2019, De Domenico et al., 2020, Patsialis et al., 2021, Masnata et al., 2021, Talley et al., 2021, Fahimi Farzam and Hojat Jalali, 2022, Chen et al., 2023).

The positive results from these studies have encouraged the use of inerter-based damping devices for mitigating seismic responses of modern wind turbines. Zhang et al. (2019) proposed a design optimization method for a tuned parallel inerter mass system (TPIMS) consisting of a tuned mass, a spring, and a parallel inerter subsystem. At a given mass ratio, the device was found to outperform a traditional TMD in its capability to reduce the tower top displacement, base shear, and bending moments experienced under seismic motion. Chen et al. (2023) employed a H_2 optimization method to optimise an inerter-based dynamic vibration absorber (IDVA) in the tower top of NRELs 5-MW wind turbine under seismic acceleration. The inerter device allowed for similar control responses to that of a TMD while having a much-decreased device mass ratio. Li et al. (2023) used a finite element model with shake table results to demonstrate the ability of a tuned inerter eddy current damper (TIECD) to reduce seismic responses. The TIECD is composed of a ball screw, a conductor, permanent magnets, and a back iron. This framework allows the device to be operated with no physical contact between components giving it an advantage over traditional inerters providing a more reliable device. Zhang et al. (2023) modified the Fast v8 code to implement a tuned mass damper inerter in NRELs 5-MW wind turbine. An extensive time domain analysis was performed to assess its seismic performance. It was found that by introducing the inerter to the system tower top displacements were reduced by up to 33% while the device stroke decreased by 71% compared to a traditional TMD.

The above literature has demonstrated the potential for reductions in wind turbine responses that can be achieved as a result of installing inerter damping devices in the nacelles of modern wind turbine towers under seismic excitation. The advantages of the mass amplification effect that arise by introducing an inerter into damping devices such as the TMD have been clearly illustrated. However, in the above literature, little work has been carried out with regard to the potential use of TMDIs for the reduction of seismic fragility of large modern multi-mega-watt wind turbines. In this paper, we address this gap in knowledge by performing a seismic fragility analysis of the IEAs 15-MW reference wind turbine with a TMDI installed in the nacelle. The wind turbine has been modelled using the finite element software Abaqus. A fragility analysis has been carried out subjecting the turbine to ground motion accelerations of various magnitudes and frequency contents comparing the damping effects of both a TMD and a TMDI.

2. Method

This section details the steps carried out in order to perform a fragility analysis of the IEA 15-MW offshore wind turbine using a finite element model. The model was developed from a crude simplistic model into a finalised complex model consisting of over 100,000 elements. Once the final model of the turbine was obtained two types of analysis were performed. First a modal analysis was executed allowing for the natural frequencies of the tower and blades to be obtained ensuring the accuracy of the model. Following this a seismic analysis was carried out, testing the turbine's fragility under seismic motion using accelerations from ground motion time histories of recorded earthquakes.

2.1. 15-MW Details

In March 2020, the International Energy Agency (IEA) in association with the National Renewable Energy Laboratory (NREL) released the design and specifications of a state-of-the-art 15-megawatt offshore reference wind turbine (Gaertner et al., 2020). The 15-megawatt wind turbine is a three-bladed upwind turbine with a hub height of 150 meters and a rotor diameter of 240 meters which is capable of producing 77.4 GWh annually. The wind turbine is a collective pitch-variable speed wind turbine enabling the wind turbine to operate over a range of rotor speeds which can be controlled by the single pitch angle of the three blades. The specifications of the turbine are depicted in the following table as defined by the IEA.

Table 1. IEA 15-MW Wind Turbine Specifications. (Gaertner et al., 2020)

Parameter	*Value*
Turbine class	IEC Class 1B
Specific rating	332W/m^2
Rotor orientation	Upwind
Number of blades	3
Rotor diameter	240m
Hub height	150m
Blade length	117m
Blade mass	65,250 kg
Root diameter	5.2m
Max chord	5.77m
Tip prebend	4m
Precone	4 deg
Cut-in wind speed	3m/s
Rated wind speed	10.59m/s
Cut-out wind speed	25m/s
Design tip-speed ratio	90
Minimum rotor speed	5rpm
Maximum rotor speed	7.56rpm
Maximum tip speed	95m/s
Design tip-speed ratio	9
First blade flapwise natural frequency	0.555 Hz
First blade edgewise natural frequency	0.642 Hz
First tower + blades natural frequency	0.17 Hz
Shaft tilt angle	6 deg
Rotor nacelle assembly mass	1,017t
Transition piece height	15m
Monopile embedment depth	45m
Monopile base diameter	10m
Tower mass	860t
Monopile mass	1,318t

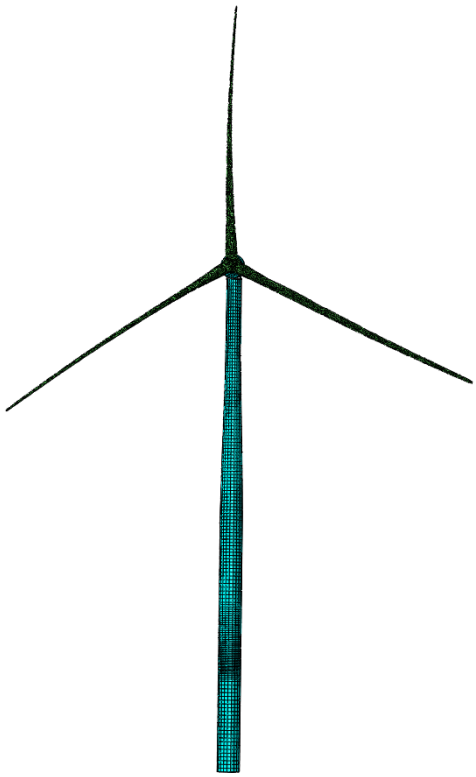

Figure 1 IEA 15-MW Wind turbine

2.2. Finite Element Model

A finite element model of the 15-MW wind turbine has been constructed using Abaqus software consisting of geometric parts provided by the IEA which were converted to be suitable for use in Abaqus. This model details parts such as flanges, bearings, the yaw system, and the bedplate providing a geometrically accurate representation of the turbine. The material and mass properties of each part were allocated as prescribed in the IEA definition of the wind turbine (Gaertner et al., 2020). The wind turbine was modelled as a fixed base turbine with fixed boundary conditions applied at the mudline. On account of the complex geometry of the wind turbine's blades and hub, it was required to implement C3D4 elements in these regions due to this element's geometric versatility. As this study focuses on the fragility of the turbine tower, this element was capable of achieving the key properties required of these regions including the natural frequency and mass distribution. All of the remaining parts have been meshed using hexahedral (brick) elements of type C3D8R, an eight-node brick element with reduced integration preventing the effects of shear locking. This element has decreased accuracy in comparison with non-linear brick elements however the computational effort required by this element is much reduced which is a critical factor when carrying out dynamic finite element simulations. Local seeding has been implemented in the transition piece of the wind turbine tower in an effort to increase the accuracy of the stresses induced in this region of interest. The element size surrounding the mud line of the tower is decreased with a single bias in the direction of the mud line as can be seen in figure 3. Structural damping was introduced to the model using Rayleigh mass proportional damping. Each material used in the turbine was assigned alpha and beta values corresponding to the influence of the mass and stiffness of the material on the damping respectively. The IEA outlined the critical damping of the turbine tower as 1% while the blades and the nacelles components were defined as having critical damping ratios of 3% and 5% respectively (Gaertner et al., 2020).

Following the completion of the model, a modal analysis of the uncontrolled wind turbine was carried out calculating the natural frequencies and mode shapes of the structure. For the dynamic simulations, the seismic ground accelerations are applied to the structure for three cases: Uncontrolled- without a damping device, TMD- with a classical TMD installed at the top of the tower, and TMDI- with a TMDI installed at the top of the tower. Due to the pre-existing natural aerodynamic damping that arises due to the turbine's blades in the fore-

aft direction, the damping devices are tuned to mitigate tower vibrations in the less damped side-to-side direction where there is a possibility of a prolonged vibration response. Boundary conditions have been implemented so that no vertical movement is allowed for the damping devices while also restraining the device in the fore-aft direction. The mass ratio of the dampers was selected to be $\mu = 0.01$, resulting in a 21,780 Kg mass. There are numerous theoretical and empirical expressions available in the literature for the evaluation of the optimal damping ratio of TMD devices such as those formulated by Ghosh and Basu (2007), Hoang et al. (2008) and Luft (1979). In this work the Den Hartog (1985) expression for the optimal TMD damping ratio is selected:

$$\zeta = \sqrt{\frac{3\,\mu}{8(1+\mu)}} \tag{1}$$

The spring stiffness of the TMD was then calculated using the following equation: $K = \omega^2 m$ where ω is the first angular frequency of the turbine and m is the mass of the TMD. The damping coefficient of the dashpot is then calculated using the following equation: $c = 2\,\zeta\omega m$. The optimum tuning parameters for the TMDI device were found as per Fitzgerald et al. (2023) with a mass ratio of $\mu = 0.01$ and an inertance of $\beta = 0.4$.

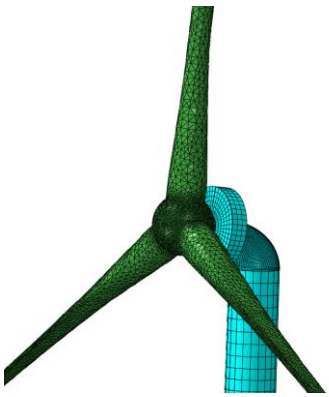

Figure 2 Detailed Mesh of Hub Blades and Rotor

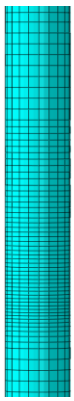

Figure 3 Tower Local Seeding

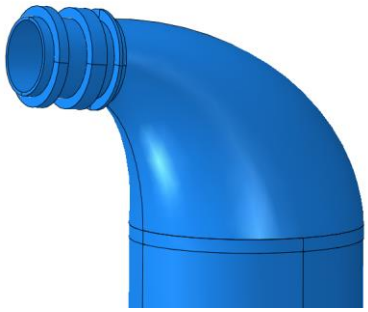

Figure 4 Detailed Bearings

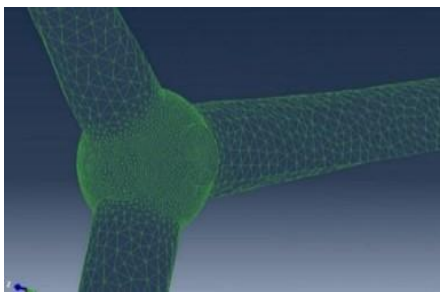

Figure 5 Hub and Blades Mesh

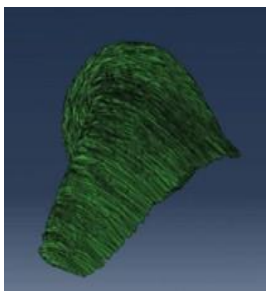

Figure 6 Blade Mesh

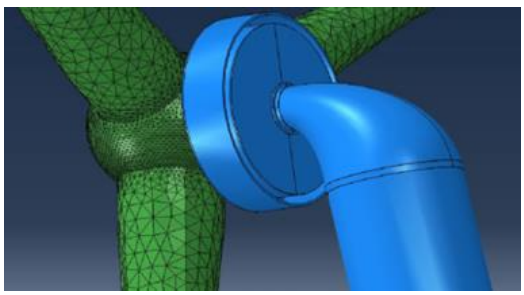

Figure 7 Detailed Bedplate, Rotor and Stator

2.3. Seismic Analysis

Three contrasting ground motions were selected from the FEMAP695 report by the Applied Technology Council (ATC, 2009). These records represented very strong far-field ground motions with magnitudes greater than 6.5 and peak ground accelerations greater than 0.2g. The response acceleration spectra of the unscaled records are compared in figure 8. All three records represent the typical case in which spectral accelerations at the first tower natural frequency of 0.17 Hz (T = 6s approx) and the first flapwise and edgewise blade natural frequencies of 0.555 Hz and 0.642 Hz (T = 1.6s approx.) are low. The three lowest tower and blade mode shapes are illustrated in figures 10-15; the natural periods of the 2nd and 3rd modes in each case lie in the region of greatest spectral acceleration (T < 1s). A detailed finite element model is required to represent these modal properties accurately and to capture the dynamic interaction of blade and tower vibration. To induce both flapwise and edgewise blade vibration, each record was applied at the fixed base of the tower as an acceleration time history with components in both the fore-aft and side-to-side directions. Asareh et al. (2016), Yuan et al. (2017) and Katsanos et al. (2017) suggest that the influence of wind loading on the dynamic response of the wind turbine is low in comparison with the seismic loads, thus wind loading was omitted from

the analysis to allow the seismic effects to be examined closely. Similarly Del Campo and Pozos-Estrada (2020) and Yuan et al. (2017) found that the seismic response of the turbine increased when the turbine was in the parked condition, thus this condition was conservatively modelled in all seismic analyses in this work. Incremental dynamic analysis was performed with all ground motion records scaled to PGAs in the range 0.2g - 0.8g. The response was simulated for the duration of each seismic event plus an additional 10 seconds.

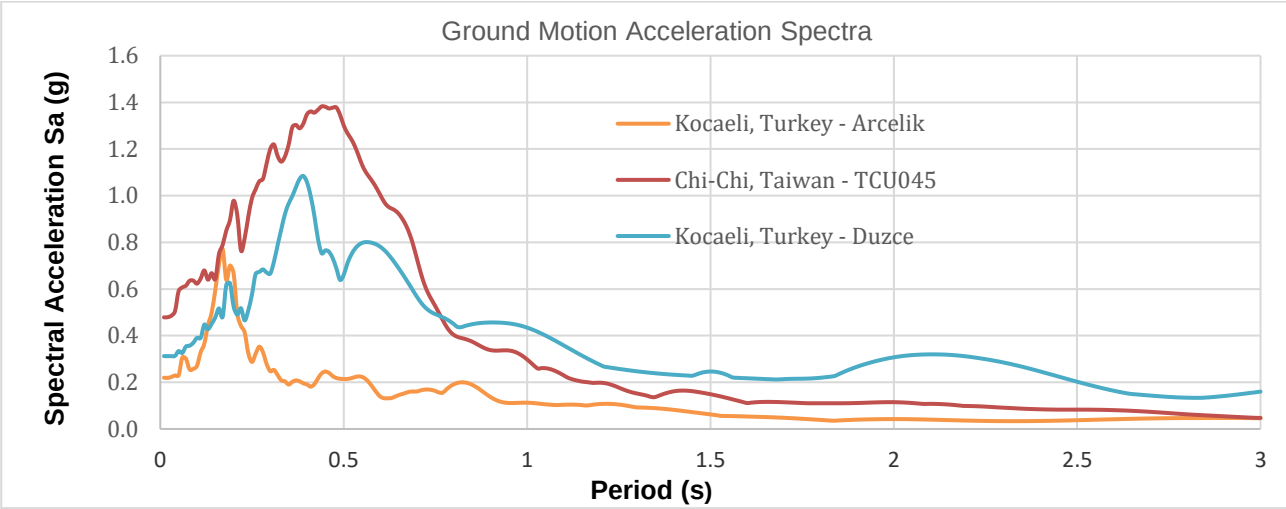

Figure 8 Ground Motion Acceleration Spectra

2.4. Limit states

Six Engineering Demand Parameters (EDP) or limit states are selected, and fragility curves are computed for each of these using the time-history analysis results. The first two limit states relate to the material of the turbine tower. These are selected as the yield stress and ultimate stress of the turbine tower steel. The tower and transition piece are proposed to be constructed with ASTM A572 Grade 50 Steel, this material has an ultimate tensile strength of 450 MPa and a tensile yield strength of 345 MPa which act as limit states 1 and 2 respectively. Sutherland (1999) describes wind turbines as fatigue-critical machines, while the ASM handbook - Failure Analysis and Prevention defines fatigue as “the phenomenon leading to fracture under repeated or fluctuating stresses having a maximum value less than the tensile strength of the material” (Powell and Mahmoud, 1986). Recognising this vulnerability, the third and fourth limit states represent fatigue failure, with stress values of 40% of the yield and ultimate limit states being selected, similar to that implemented by Zuo et al. (2020). The firth limit state was also calculated according to Zuo et al. (2020) who defined a serviceability limit state (SLS) for the 5-MW NREL turbine tower in the roll degree of freedom as $0.5°$. This $0.5°$ limit arises from DNV guidelines (DNV et al., 2014) which incorporates construction errors of up to $0.25°$. This corresponds to a 1.29m displacement at the top of the tower for the 15-MW turbine considered in this study. The final limit state was selected due to the sensitivity of wind turbines to the acceleration of the nacelle. Dueñas-Osorio and Basu (2008) conducted a study on wind turbine unavailability as a function of wind-induced vibration of the tower. This study found that the vibrations of the tower can result in the malfunction of acceleration-sensitive equipment which is typically housed in the nacelle of the wind turbine. The faults that can arise in this equipment lead to disruptions in power production, which is unacceptable in post-hazard conditions. Kaynia et al. (2023) suggested a maximum acceleration of 0.2g at the tower top as a common industrial standard and this is adopted as the sixth limit state in this study.

2.5. Fragility Analysis

The fragility curves in this study have been produced following an approach developed by Baker (2015), with the fragility function defined as:

$$\mathbf{p}(\mathbf{C}|\mathbf{IM}=\mathbf{x}) = \Phi\left(\frac{ln(x/\theta)}{\beta_f}\right) \tag{2}$$

where $\mathbf{p}(\mathbf{C}|\mathbf{IM}=\mathbf{x})$ is the probability that x, a seismic ground motion, will cause the wind turbine to exceed C, a defined limit state. In Equation 2, Φ is the normal cumulative distribution function, θ and β_f are the fragility

parameters; the median of the fragility function and the standard deviation of $\ln(IM)$ respectively. The intensity measure (IM) in this case is the peak ground acceleration (PGA) of the seismic record. The Maximum Likelihood Estimation (MLE) is used to find the best estimate of the fragility parameters (Baker, 2015):

$$\textbf{Likelihood} = \prod_{j=1}^{m} \binom{n_j}{z_j} p_j^{z_j} (1-p_j)^{n_j - z_j} \tag{3}$$

$\prod$ is the product of the sequence, m is the number of PGA ranges, n_j is the number of seismic ground acceleration records implemented for a given PGA range, and z_j is the number of instances where the limit state is exceeded under these ground motions. By substituting equation 2 into equation 3 the following formula is produced:

$$\textbf{Likelihood} = \prod_{j=1}^{m} \binom{n_j}{z_j} \times \Phi\left(\frac{ln(x_j/\theta)}{\beta_f}\right)^{z_j} \times \left[1 - \Phi\left(\frac{ln(x_j/\theta)}{\beta_f}\right)^{(n_j - z_j)}\right] \tag{4}$$

By maximising the likelihood function, the best estimate of the fragility parameters can be obtained:

$$\hat{\theta}, \widehat{\beta_{\mathbf{f}}} \;=\; arg\max_{(\theta,\beta_f)} \sum_{j=1}^{m} \left\{ ln\binom{n_j}{z_j} + z_j \ln\Phi\left(\frac{ln(x_j/\theta)}{\beta_f}\right) + (n_j - z_j) \ln\left[1 - \Phi\left(\frac{ln(x_j/\theta)}{\beta_f}\right)\right] \right\} \tag{5}$$

3. Results

3.1. Model Benchmark

Modal analysis was performed in order to verify the finite element model. The first natural frequency obtained in this analysis matches identically that specified by the IEA at 0.17 Hz (Gaertner et al., 2020). Additionally, in figure 9, the first mode shape of the tower in the side-side direction is compared against the IEA-specified mode shape from their OpenFAST software and shows good agreement, thus further verifying the model. Figures 10-12 present the first three mode shapes of the turbine tower, while the first three blade mode shapes are presented in figures 13-15. The natural frequencies of the turbine blades in these modes were also found to match the natural frequencies specified by the IEA.

3.2. TMDI performance assessment

Figure 16 presents results from time-history analyses with two earthquake records, specifically the computed accelerations and displacements at the top of the turbine tower. While the displacement response is dominated by the low frequency fundamental tower mode, substantial higher mode effects including blade vibration are evident in the response accelerations, particularly in the earlier strong motion phase of the earthquakes. The benefits of installing the damping devices are clearly observable with large reductions displayed in both displacement and acceleration response. The presence of the TMD reduces peak displacements, however, the TMDI can be seen to greatly outperform the traditional TMD providing greater mitigation of displacements throughout the response. An even stronger effect is observed in the acceleration time histories indicating that the TMDI has a much greater ability to reduce the peak acceleration at top of the tower providing protection to acceleration-sensitive equipment.

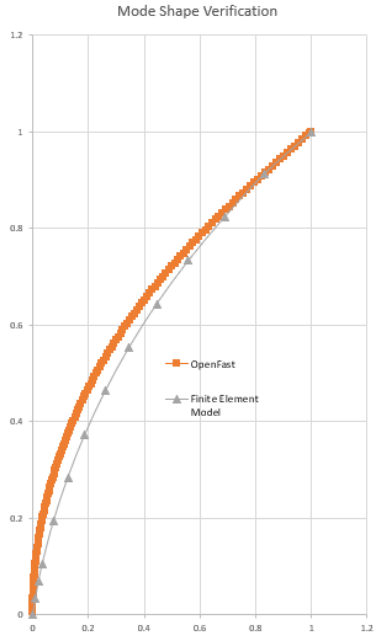

Figure 9 Tower Mode comparison

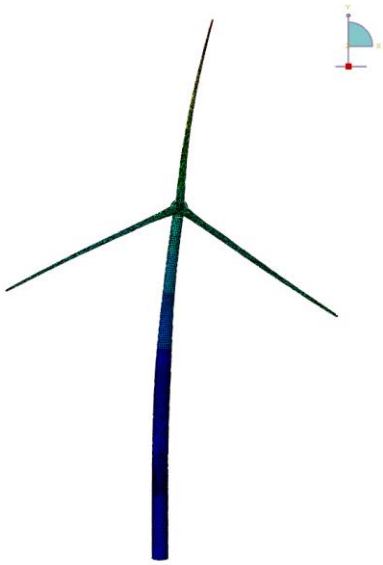

Figure 10 Tower Mode Shape: 1

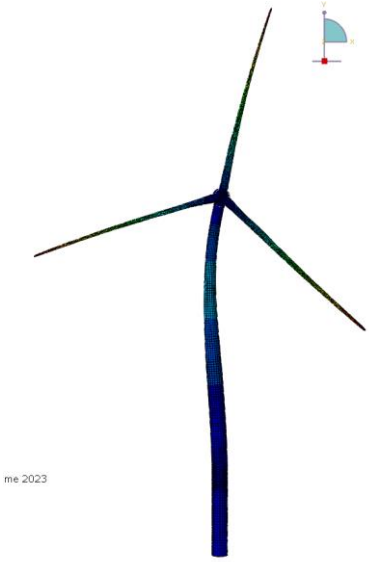

Figure 11 Tower Mode Shape: 2

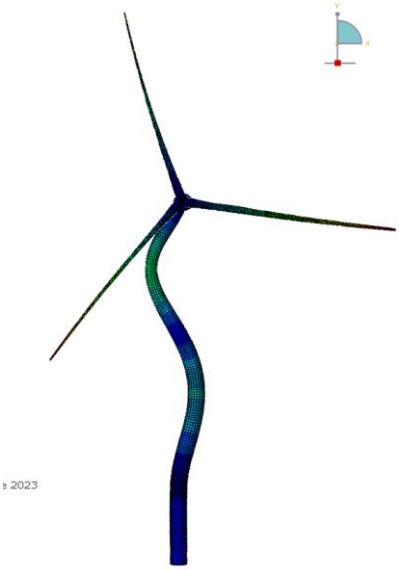

Figure 12 Tower Mode Shape: 3

Figure 13 Blade Mode Shape: 1

Figure 14 Blade Mode Shape: 2

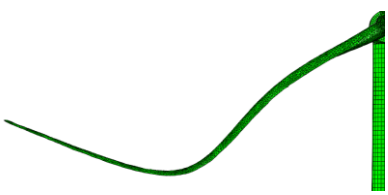

Figure 15 Blade Mode Shape: 3

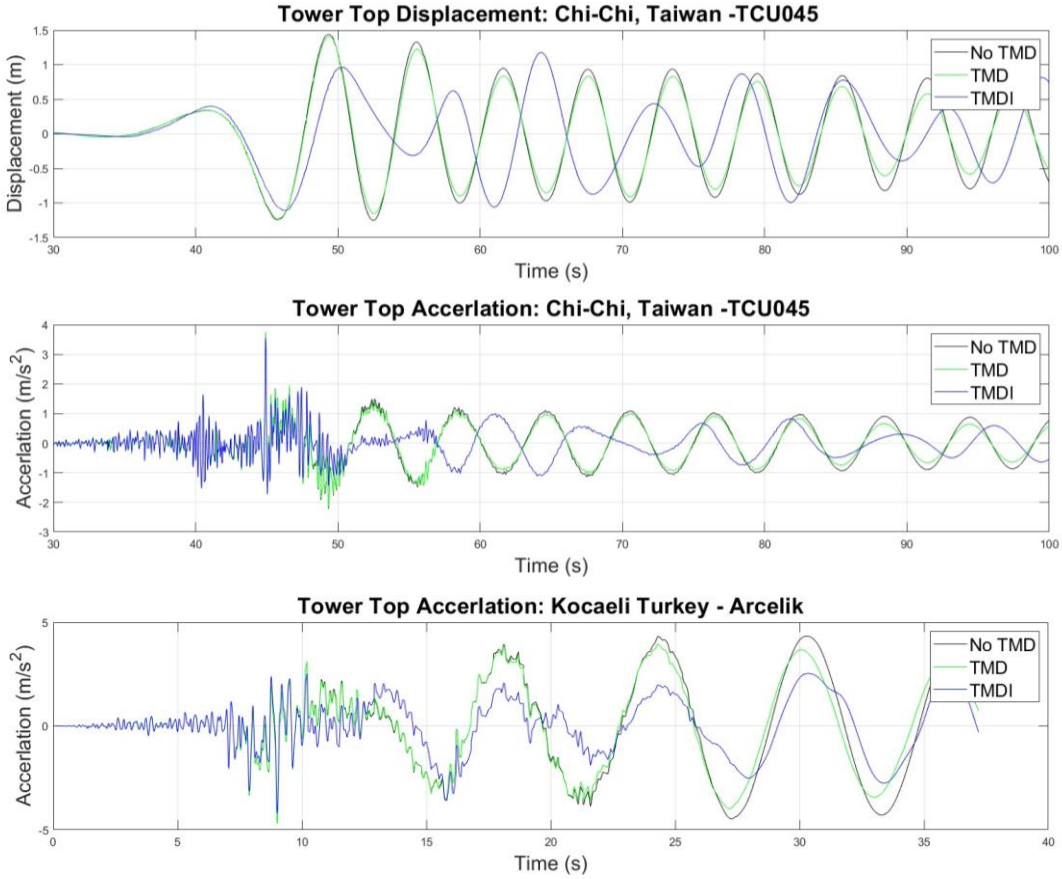

Figure 16 Effect of TMDI on Displacement and Acceleration Time History

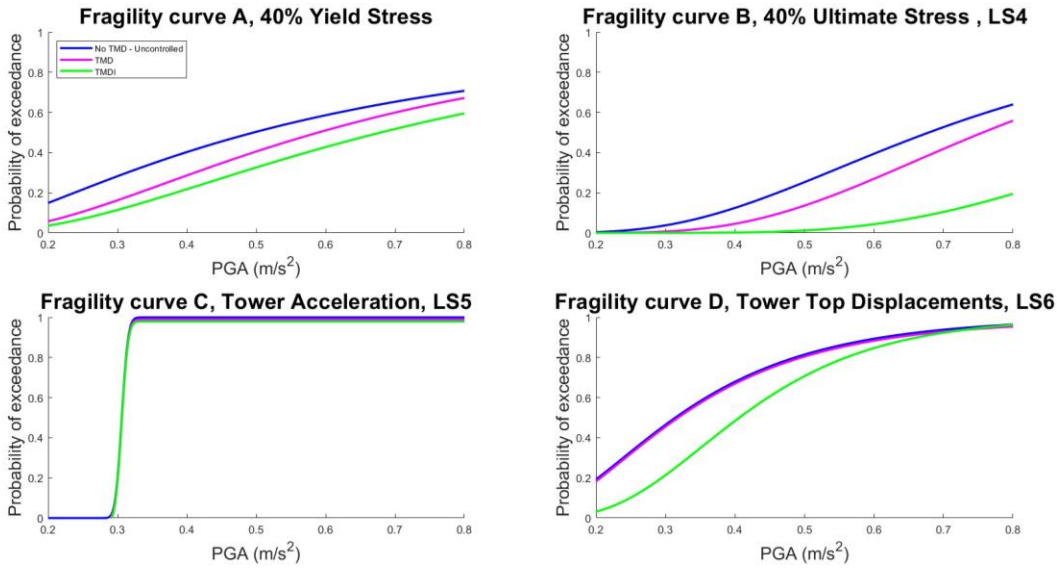

Figure 17 Fragility Curves A-D

Figure 17 illustrates the fragility curves produced using the Maximum Likelihood Estimation, for limit states 3-6. Fragility curves for limit states 1 and 2 are not presented as the yield stress was not exceeded. The largest recorded stress across the three earthquake records was 322.7 MPa, just below the yield limit of 345 MPa. This maximum stress is reduced to well below the yield stress when the TMDI installed is installed producing a maximum stress of 208.9 MPa. The benefit of installing damping devices can be clearly seen in fragility curve A relating to limit state 3 where the damping devices can be seen to reduce the fragility of the turbine over the full range of peak ground accelerations. The TMDI outperforms the TMD providing additional fragility

reductions. In fragility curve B for the ultimate stress-based limit state 4, the TMDI again outperforms the TMD with the fragility reductions of the TMDI becoming greater as the PGA increases.

The effects of the damping devices cannot be observed in fragility curve C for limit state 5 relating to acceleration-sensitive equipment in the nacelle. However, examination of peak acceleration results confirms that the TMDI outperformed the conventional TMD reducing side-to-side peak acceleration by 10%. The damping effect of the TMDI can be observed in fragility curve D relating to limit state 6 where the TMDI clearly reduces the fragility of the turbine tower. Again, examining the results in further detail, the TMDI can be seen to produce much greater response reductions than the traditional TMD. A reduction of up to 33% is observed in the peak displacement of the tower top when the TMDI is implemented in comparison with a 20% reduction for a conventional TMD.

4. Conclusion

The influence of the novel tuned mass damper inerter on the seismic response of a large modern multi-mega-watt wind turbine has been investigated. A detailed finite element model of the IEA 15-MW wind turbine was constructed and verified using modal analysis that matched both the natural frequency and mode shape to the specifications of the IEA. An inerter device was added to a traditional tuned mass damper at the top of the turbine tower to increase the control capabilities of the device. This damping device was optimally tuned for side-side tower response due to the low natural damping provided in this direction. The model was employed in time history analysis with historical earthquake ground motion records to examine the influence of the TMDI on the accelerations, displacements, and resulting stresses of the wind turbine. Fragility curves for the wind turbine subject to seismic loads were produced via the Maximum Likelihood Estimation (MLE) and used to compare the performance of a traditional TMD with that of a TMDI. The response time histories and fragility curves demonstrate the clear advantages of installing damping devices in a wind turbine tower. Fragility curves A and B illustrate the reductions that can be achieved by these devices in reducing the stresses experienced in the turbine tower. The fragility curves show that the introduction of the inerter device helps the TMDI to outperform the TMD over the full range of peak ground accelerations. Additionally, the introduction of the inerter to the TMD system greatly increases the damping device's ability to reduce the seismic response accelerations and displacements experienced by the wind turbine and as a result, increases the reliability of the turbine and its components. These findings confirm the importance of detailed finite element modelling to capture the complex 3D dynamic response of the integrated tower-blades assembly and indicate the potential for further simulations with a larger number of earthquake records and range of seismological characteristics.

In conclusion, by installing a TMDI in a turbine tower, the response of the tower induced by seismic motion will be largely decreased with a number of important benefits: the reliability of the turbine will be increased hence decreasing costly down-times and ensuring a reliable source of energy following damaging earthquakes. The accelerations in the nacelle will be reduced protecting sensitive components hence decreasing both the need and cost associated with repairs. These effects will allow turbines to produce power during times of need and allow turbines in seismic regions to operate for prolonged periods of time thus decreasing their LCOE.

5. References

Arrigan, J., Pakrashi, V., Basu, B., and Nagarajaiah, S. (2011). Control of flapwise vibrations in wind turbine blades using semi-active tuned mass dampers. Structural Control and Health Monitoring, 18(8):840–851.

Asareh, M.-A., Schonberg, W., and Volz, J. (2016). Fragility analysis of a 5-mw nrel wind turbine considering aero-elastic and seismic interaction using finite element method. Finite Elements in Analysis and Design, 120:57–67.

ATC (2009). Quantification of building seismic performance factors, fema p695.

Baker, J. W. (2015). Efficient analytical fragility function fitting using dynamic structural analysis. Earthquake Spectra, 31(1):579–599.

Chen, Q., Zhang, L., Zhang, R., Pan, C., et al. (2023). H_, 2023.

Dai, K., Huang, H., Lu, Y., Meng, J., Mao, Z., and Camara, A. (2021). Effects of soil–structure interaction on the design of tuned mass damper to control the seismic response of wind turbine towers with gravity base. Wind Energy, 24(4):323–344

De Domenico, D., Deastra, P., Ricciardi, G., Sims, N. D., and Wagg, D. J. (2019). Novel fluid inerter based tuned mass dampers for optimised structural control of base-isolated buildings. Journal of the Franklin Institute, 356(14):7626–7649.

De Domenico, D., Qiao, H., Wang, Q., Zhu, Z., and Marano, G. (2020). Optimal design and seismic performance of multi-tuned mass damper inerter (mtmdi) applied to adjacent high-rise buildings. The Structural Design of Tall and Special Buildings, 29(14):e1781.

Del Campo, J. M. and Pozos-Estrada, A. (2020). Multi-hazard fragility analysis for a wind turbine support structure: An application to the southwest of mexico. Engineering Structures, 209:109929.

Den Hartog, J. P. (1985). Mechanical vibrations. Courier Corporation.

DNV, D. N. V. et al. (2014). Design of offshore wind turbine structures. Internet Requests for Comments, DET NORSKE VERITAS AS, OFFSHORE STANDARD DNV-OS-j101.

Dueñas-Osorio, L. and Basu, B. (2008). Unavailability of wind turbines due to wind-induced accelerations. Engineering Structures, 30(4):885–893.

Dyke, S., Spencer Jr, B. F., Quast, P., and Sain, M. (1995). Role of control-structure interaction in protective system design. Journal of engineering mechanics, 121(2):322–338.

Enevoldsen, P. and Xydis, G. (2019). Examining the trends of 35 years growth of key wind turbine components. Energy for sustainable development, 50:18–26.

Fahimi Farzam, M. and Hojat Jalali, H. (2022). Tandem tuned mass damper inerter for passive control of buildings under seismic loads. Structural Control and Health Monitoring, 29(9):e2987.

Fitzgerald, B. and Basu, B. (2020). Vibration control of wind turbines: recent advances and emerging trends. Int. J. Sustain. Mater. Struct. Syst, 4:347–372.

Fitzgerald, B., Basu, B., and Nielsen, S. R. (2013). Active tuned mass dampers for control of in-plane vibrations of wind turbine blades. Structural Control and Health Monitoring, 20(12):1377–1396.

Fitzgerald, B., McAuliffe, J., Baisthakur, S., and Sarkar, S. (2023). Enhancing the reliability of floating offshore wind turbine towers subjected to misaligned wind-wave loading using tuned mass damper inerters (tmdis). Renewable Energy, 211:522–538.

Fitzgerald, B., Sarkar, S., and Staino, A. (2018). Improved reliability of wind turbine towers with active tuned mass dampers (atmds). Journal of Sound and Vibration, 419:103–122.

Gaertner, E., Rinker, J., Sethuraman, L., Zahle, F., Anderson, B., Barter, G. E., Abbas, N. J., Meng, F., Bortolotti, P., Skrzypinski, W., et al. (2020). IEA wind tcp task 37: definition of the IEA 15-megawatt offshore reference wind turbine. Technical report, National Renewable Energy Lab.(NREL), Golden, CO (United States).

Ghosh, A. and Basu, B. (2007). A closed-form optimal tuning criterion for tmd in damped structures. Structural Control and Health Monitoring, 14(4):681–692.

Hoang, N., Fujino, Y., and Warnitchai, P. (2008). Optimal tuned mass damper for seismic applications and practical design formulas. Engineering structures, 30(3):707–715.

Justin-Damien, G. K. (2022). The energy shock could sap global growth for years.

Katsanos, E. I., Sanz, A. A., Georgakis, C. T., and Th¨ons, S. (2017). Multi-hazard response analysis of a 5mw offshore wind turbine. Procedia engineering, 199:3206–3211.

Katsanos, E. I., Th¨ons, S., and Georgakis, C. T. (2016). Wind turbines and seismic hazard: a state-of-the-art review. Wind Energy, 19(11):2113–2133.

Kaynia, A. M., Blekastad, H., Schell, P., and Walter, E. L. (2023). Seismic response of floating wind turbines due to seaquakes. Wind Energy, 26(2):145–162.

Kontoni, D.-P. N. and Farghaly, A. A. (2023). Assessing seismic mitigation schemes of tuned mass dampers for monopile offshore wind turbine including pile–soil–structure interaction. Asian Journal of Civil Engineering, pages 1–27.

Lackner, M. A. and Rotea, M. A. (2011a). Passive structural control of offshore wind turbines. Wind energy, 14(3):373–388.

Lackner, M. A. and Rotea, M. A. (2011b). Structural control of floating wind turbines. Mechatronics, 21(4):704–719.

Li, D., Ikago, K., and Yin, A. (2023). Structural dynamic vibration absorber using a tuned inerter eddy current damper. Mechanical Systems and Signal Processing, 186:109915.

Li, W., Zhang, Q., Yang, Z., Zhu, Q., and Du, Y. (2020). Seismic vibration mitigation of wind turbine tower using bi-directional tuned mass dampers. Mathematical Problems in Engineering, 2020:1–22.

Luft, R. (1979). Optimal tuned mass dampers for buildings. Journal of the Structure Division, ASCE, 105:2766 – 2772.

Martin del Campo, J. O., Pozos-Estrada, A., and Pozos-Estrada, O. (2021). Development of fragility curves of land-based wind turbines with tuned mass dampers under cyclone and seismic loading. Wind Energy, 24(7):737–753.

Masnata, C., Di Matteo, A., Adam, C., and Pirrotta, A. (2021). Assessment of the tuned mass damper inerter for seismic response control of base-isolated structures. Structural Control and Health Monitoring, 28(2):e2665.

Mo, R., Kang, H., Li, M., and Zhao, X. (2017). Seismic fragility analysis of monopile offshore wind turbines under different operational conditions. Energies, 10(7):1037.

Murtagh, P., Ghosh, A., Basu, B., and Broderick, B. (2008). Passive control of wind turbine vibrations including blade/tower interaction and rotationally sampled turbulence. Wind Energy: An International Journal for Progress and Applications in Wind Power Conversion Technology, 11(4):305– 317.

Patsialis, D., Taflanidis, A., and Giaralis, A. (2021). Tuned-mass-damper-inerter optimal design and performance assessment for multi-storey hysteretic buildings under seismic excitation. Bulletin of Earthquake Engineering, pages 1–36.

Powell G. W. and Mahmoud, S. E. (1986). Metals handbook, volume 11–failure analysis and prevention. American Society for Metals, Metals Park, Ohio 44073, USA, 1986. 843.

Prowell, I., Elgamal, A.-W. M., and Jonkman, J. M. (2010). FAST simulation of wind turbine seismic response. National Renewable Energy Laboratory.

Sarkar, S. and Chakraborty, A. (2018). Optimal design of semiactive mr-tlcd for along-wind vibration control of horizontal axis wind turbine tower. Structural Control and Health Monitoring, 25(2):e2083.

Si, Y., Karimi, H. R., and Gao, H. (2013). Modeling and parameter analysis of the oc3-hywind floating wind turbine with a tuned mass damper in nacelle. Journal of Applied Mathematics, 2013.

Smith, M. C. (2002). Synthesis of mechanical networks: the inerter. IEEE Transactions on automatic control, 47(10):1648–1662.

Stewart, G. M. and Lackner, M. A. (2014). The impact of passive tuned mass dampers and wind–wave misalignment on offshore wind turbine loads. Engineering Structures, 73:54–61.

Sutherland, H.J., 1999. On the fatigue analysis of wind turbines.

Talley, P. C., Javidialesaadi, A., Wierschem, N. E., and Denavit, M. D. (2021). Evaluation of steel building structures with inerter-based dampers under seismic loading. Engineering Structures, 242:112488.

Yeter, B., Tekgoz, M., Garbatov, Y., and Guedes Soares, C. (2020). Fragility analysis of an ageing monopile offshore wind turbine subjected to simultaneous wind and seismic load. Safety in Extreme Environments, 2:155–170.

Yuan, C., Chen, J., Li, J., and Xu, Q. (2017). Fragility analysis of large-scale wind turbines under the combination of seismic and aerodynamic loads. Renewable Energy, 113:1122–1134.

Zhang, R., Zhao, Z., and Dai, K. (2019). Seismic response mitigation of a wind turbine tower using a tuned parallel inerter mass system. Engineering Structures, 180:29–39.

Zhang, T., Wang, W., Li, X., and Wang, B. (2023). Vibration mitigation in offshore wind turbine under combined wind-wave-earthquake loads using the tuned mass damper inerter. Renewable Energy, 216:119050.

Zhao, B., Gao, H., Wang, Z., and Lu, Z. (2018). Shaking table test on vibration control effects of a monopile offshore wind turbine with a tuned mass damper. Wind energy, 21(12):1309–1328.

Zuo, H., Bi, K., and Hao, H. (2017). Using multiple tuned mass dampers to control offshore wind turbine vibrations under multiple hazards. Engineering Structures, 141:303–315.

Zuo, H., Bi, K., Hao, H., Xin, Y., Li, J., and Li, C. (2020). Fragility analyses of offshore wind turbines subjected to aerodynamic and sea wave loadings. Renewable Energy, 160:1269–1282.